ChemComm

Accepted Manuscript

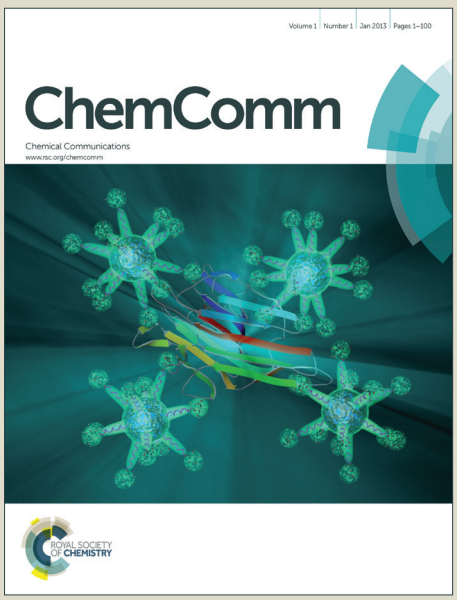

ROYAL SOCIETY OF CHEMISTRY

www.rsc.org/chemcomm

Journal Name

RSCPublishing

COMMUNICATION

Site-Specific Fluorescence Spectrum Detection and Characterization of hASIC1a Channels upon Toxin Mambalgin-1 binding in Live Mammalian Cells

Cite this: DOI: 10.1039/x0xx00000x

Received 00th January 2012,
Accepted 00th January 2012

DOI: 10.1039/x0xx00000x

www.rsc.org/

Ming Wen‡, Xiaoqi Guo‡, Peibei Sun, Liang Xiao, Juan Li, Ying Xiong, Jin Bao, Tian Xue, Longhua Zhang*, Changlin Tian*

The synthesis of fluorescent unnatural amino-acid Anap was optimized and the Anap was incorporated into four sites in acid-pocket or transmembrane region of human acid-sensing ion channel-1a (hASIC1a). Combinational Anap fluorescence spectra and patch-clamp electrophysiology data illustrated site-specific conformational responses upon toxin mambalgin-1 binding. This combinational approach can be used to analyse conformational properties of many different eukaryotic proteins in their functional states, in a site-specific manner in live mammalian cells.

Fluorescent probe labeling of proteins is emerging as a frequently used method for protein localization, functional characterization, cell biology and high resolution cellular imaging studies. The general method involves attaching the target protein to a fluorescent protein[1] or fusion tag specifically coordinating a dye compound.[2] However, the large size of fluorescent proteins or fusion tags (>20 kDa), and the typical requirements for C- or N-terminal fusion partners set limits for functional and structural studies of proteins *in vitro* and *in vivo*.[3] Recently, an alternative approach was developed for incorporating a small unnatural amino acid (UAA) (<250 Da) into the target protein in a site-specific manner, using the orthogonal tRNA/aminoacyl-tRNA synthetase (RS) pair.[4] Several different unnatural amino acids were incorporated into amber nonsense codon sites, including 7-hydroxycoumarin, dansyl side chains, and amino-naphthalene derivatives in *Escherichia coli*, *Saccharomyces cerevisiae*, and mammalian cells, respectively.[4b, 5] The successful site-specific incorporation of environment-sensitive 3-(6-acetylnaphthalen-2-ylamino)-2-amino propanoic acid (Anap) in target proteins has greatly facilitated functional and structural studies of eukaryotic proteins in live mammalian cells[4a], which is superior to site-specific NMR analysis of proteins' conformation or dynamics due to its high sensitivity and easier incorporation in mammalian cell system[6].

Ion channels are pore-forming membrane proteins that transport ions across the membrane, and these proteins can be regulated by stimuli such as voltage, ligands, auxiliary proteins, temperature and mechanical stress. Ion channel regulation has been extensively investigated using various biophysical methods. Fluorescence labeling was used to probe conformational changes in the region surrounding the fluorophore that lead to changes in the microenvironment and hence emission spectra.[7] For *in vivo* site-specific fluorescence analysis of ion channels, fluorophores can be coupled to the sulfhydryl group of naturally occurring or introduced cysteine residues. However, only surface-exposed residues in the extracellular domains of ion channels can be analyzed using the cysteine-based site-specific fluorophore incorporation method.[8] Recently, the fluorescent UAA Anap was incorporated into a voltage gated K^+ channel in a site-specific manner to facilitate the study of the dynamic internal pore opening in oocyte cells[9]. However, the oocyte system could not provide suitable condition for structure-function correlation studies of general eukaryotic proteins (especially soluble proteins or membrane proteins other than ion channels).

Site-specific incorporation of a small UAA such as Anap can in principle facilitate the site- and protein-specific characterization of eukaryotic ion channels in live mammalian cells using combined fluorescence visualization and confocal microscopy. However, most of the combinational studies can only provide information of fluorescence intensity. Despite of high signal intensity (quantum yield of 0.48 in ethanol), Anap has demonstrated high sensitivity to solvent polarity with a significant shift in emission maximum (λ^{max}_{em}) on transitioning from water (490 nm) to ethyl acetate (420 nm).[4b] Therefore, changes in Anap fluorescence spectra, especially red- or blue-shifting of λ^{max}_{em}, could be used to probe conformational changes or microenvironment variations in the vicinity of the incorporated UAA. To this end, Anap flurescence spectra were collected using an additional prism-based monochromator prior to emission signal acquisition (Fig. 1A). This approach might be superior to standard fluorescence intensity detection, as is often used in voltage clamp fluorometry (VCF) studies on ion channels.[7a]

Human acid sensing ion channels (hASIC) are proton-gated cation channels in neuronal system associated with nociception,

fear, depression, seizure and degeneration, suggesting roles in pain, neurological and psychiatric disorders[10]. Inhibition of hASIC therefore emerges as a new potential therapeutic strategy with huge physiological and pharmaceutical significance. Mambalgin-1 is a cysteine rich, 57 residue polypeptide isolated from the venom of black mamba snakes, which was demonstrated to abolish pain through inhibition of hASIC in central or peripheral neurons.[11] Recently, the toxin was chemically synthesized and the structure was determined[12], however, no detail mechanism studies on hASIC's response to the mambalgin-1 binding were reported yet, except some recent mutagenesis studies[12a, 13]. Here, Anap was site-specifically incorporated into hASIC1a expressed in mammalian CHO cells to facilitate conformational analysis upon mambalgin-1 binding. We started with the Anap synthesis optimization upon previous protocols, which was modified to initiate from the readily accessible compound 2-bromonaphthalene (Fig. 1B). Following Friedel-Crafts acetylation to generate 2-acetyl-6-bromonaphthalene,[14] a Fukuyama-Mitsunobu reaction was performed that achieved the final product Anap.[15] A total of 8 steps and 10 days were required for the entire synthesis, and each step was optimized to ensure mild conditions and the highest possible yield. Apart from the relatively low-yielding first step (35%), all other steps gave yields between 73–97%, giving a final yield of 20.7% from 2-bromonaphthalene (for experimental details, see the Supporting Information).

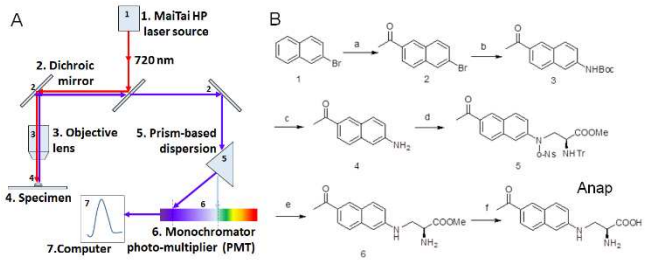

Figure 1. (A) Schematic illustration of the two-photon excitation and spectrum acquisition using confocal microscopy. A prism-based monochromator was set up before the photo-multiplier. (B) Synthesis of Anap starting from 2-bromonaphthalene. Reagents, conditions and yields are shown (a) AcCl, $AlCl_3$, $PhNO_2$, 100°C, 5 h, 35%; (b) Boc-NH_2, CuI, DMEDA, K_2CO_3, toluene, 110 °C, 30 h, 71%; (c) TFA, DCM, rt, 3 h. 95%; (d) i,o-NsCl, pyridine, DCM, rt, overnight; ii, N-Trt-Ser-OMe, DIAD, PPh_3, toluene, rt, overnight, 88% over two steps; (e) i, TFA, DCM, H_2O, rt, 4 h; ii, PhSH, K_2CO_3, DMF, rt, 3 h, 73% over two steps; (f) 2 M HCl, 60°C, 8 h, 97%.

To implement site-specific functional characterization of hASIC1a in live mammalian cells, fluorescence spectra of Anap-labeled hASIC1a channels expressed in CHO cells were collected using two-photon excitation (excitation: 720 nm, two-photon; emission: 380–550 nm), with Anap incorporations at different sites of hACIS1a, in the absence or presence of mambalgin-1 (at different toxin concentrations). Four sites were chosen for the fluorescent spectra analysis: T236, D347, Y68 and F69. The first two sites were located in the extracellular domain, close to the acid-pocket region which can sense the pH gating or toxin binding, while the latter two were located in the transmembrane domain, reflecting the conformational responses of the channel upon ligand binding[16]. Shown in Figure 2 were the Anap fluorescence spectra for hASIC1a-T236Anap and hASIC1a-D347Anap. Both of the two Anap incorporation sites were located in the hASIC1a acid-pocket region (Fig. 2A) and predicted for mambalgin-1 binding.[12a, 17] The Anap fluorescence image of CHO cells expressing hASIC1a-T236Anap and hASIC1a-D347Anap displayed a blue color in the cell envelope under confocal microscopy, which confirmed that the hASIC1a proteins were correctly trafficked to the cell plasma membrane (Fig. 2B, 2C). The observed various fluorescence intensities of hASIC1a with Anap incorporation in different cells were probably due to different transfection efficiency of the plasmids. The acquired Anap fluorescence spectra of hASIC1a-T236Anap in the CHO membrane region demonstrated a minor intensity attenuation upon perfusion of 500 nM mambalgin-1 (Fig. 2B), but it was difficult to estimate the λ^{max}_{em} shift due to the relatively large measurement errors. However, λ^{max}_{em} red shifting (from 463 nm to 470 nm) and pronounced intensity attenuations were observed for hASIC1a-D347Anap upon perfusion of increasing mambalgin-1 concentrations (Fig. 2C). Furthermore, a sigmoid curve was fitted to the Anap fluorescence intensities at λ^{max}_{em} versus mambalbin-1 concentration (Fig. 2D). The observed dose-dependent response verified the direct correlation between toxin binding and changes in the environment surrounding the D347Anap site.

With the aid of blue Anap fluorescence images of CHO cells expressing the labeled channels, Anap fluorescence spectra were also acquired for the same cells expressing hASIC1a-Y68Anap (Fig. 3A) or hASIC1a-F69Anap (Fig 3C) in the absence or presence of 500 nM mambalgin-1. These Anap incorporation sites are located in transmembrane helix 1 (TM1; Y68Anap, F69Anap)[16-17] (Fig. 3C). A pronounced intensity drop was observed in the Anap fluorescence spectra for hASIC1a-Y68Anap upon toxin perfusion (Fig. 3A), while no obvious Anap fluorescence spectra changes were observed for hASIC1a-F69Anap. The observations indicated that there might be conformational changes in the Y68Anap site upon toxin binding, but not in the F69Anap site.

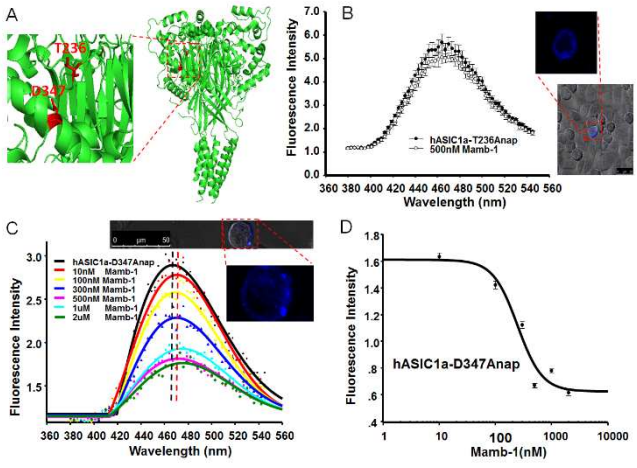

Figure 2. Fluorescence spectrum acquisition of Anap incorporation at the acid-pocket region of hASIC1a expressed in CHO cells at pH 7.4. (A) Structural model of hASIC1a, based on the crystal structure of chicken ASIC1 (PDB: 3S3W), with the two mutation sites (T236 and D347) and their side-chain orientations shown. (B) Fluorescence spectra of hASIC1a-T236Anap in the absence or presence of 500 nM mambalgin-1, and fluorescence image of the recording cell (right, bar scale: 50 μm). (C) Fluorescence spectra of hASIC1a-D347Anap in the absence or presence of mambalgin-1 at the indicated

concentrations. The solid lines on the spectrum and fluorescence image are fitted to the Weibull equation (right, bar scale: 50 μm). (D) Maximum fluorescence intensities of hASIC1a-D347Anap with different concentrations of mambalgin-1, as shown in (C). The solid line was fitted to the Hill equation fit to estimate the mambalgin-1 dose-dependent response.

In order to correlate the Anap fluorescence spectra of different UAA incorporation sites, single-cell patch-clamp electrophysiology studies were conducted. Similarly as wild type hASIC1a, the normalized current of the four mutants with Anap incorporation demonstrated pH gating channel conductance, despite exhibiting different pH sensitivities (Fig. 4A). In hASIC1a with Anap incorporated at either of the TM1 sites (Y68Anap, F69Anap), there was a shift in the pH gating mid-point from 6.59 to around 6.15, whereas the pH gating mid-point of hASIC1a with Anap incorporated in the acid-pocket region (T236Anap, D347Anap) were shifted to around 5.60. We were curious as to why similar pH gating mid-point shifts at the same regions led to different Anap fluorescence intensity attenuations. To correlate channel functional and fluorescence-based structural analysis, the channel conductance at different mambalgin-1 concentrations was measured for the four Anap-labeled hASIC1a proteins (Fig. 4B). Current attenuations upon increasing mambalgin-1 were observed for all four mutant channels (Fig. 4C, 4D).

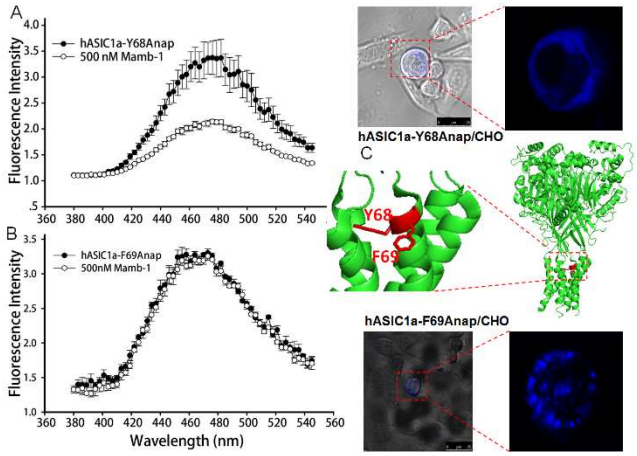

Figure 3. Fluorescence spectra acquisition of Anap incorporation at transmembrane helix 1 of hASIC1a expressed in CHO cells at pH 7.4. (A) Fluorescence spectra of hASIC1a-Y68Anap in the absence or presence of 500 nM mambalgin-1, and a fluorescence image of the recording cell (right, bar scale: 50 μm). (B) Fluorescence spectra of hASIC1a-F69Anap in the absence or presence of 500 nM mambalgin-1, and a fluorescence image of the recording cell (right, bar scale: 50 μm). (C) Structural model of hASIC1a showing the two mutated sites (Y68 and F69) and their side-chain orientations.

For the two mutants with Anap labeling at TM1, the measured IC_{50} of hASIC1a-F69Anap (163.33 nM) was similar as the wild type channel (150.87 nM, pH 6.0), whereas the hASIC1a-Y68Anap mutant differed markedly (90.09 nM). From previous structural studies, it is known that the two TM1 sites are further away from the toxin binding region, but TM1 is essential for channel opening/closing and for cation conductance.[16-17] Therefore, the correlation between the Anap fluorescence intensity attenuation upon mambalgin-1 binding (Fig. 3A) and the mambalgin-1 dose dependent IC_{50} variation of the wild type channel (Fig. 4C) indicated potential conformational changes at the Y68 site upon the mambalgin-1 binding. This is consistent with the crystal structure, which shows that Y68 lines the channel pore, and F69 is a lipid-facing residue (Fig. 3C).

For the two mutants labeled in the acid-pocket region, the measured IC_{50} of hASIC1a-T236Anap (220.65 nM) and D347Anap (128.48 nM) were significantly different from the wild type channel (580.20 nM, pH 5.0). Previous studies indicated that the acid-pocket region is also the toxin binding site, and mambalgin-1 binding may lead to desensitization, resulting in deceased cation conductance.[11a] Therefore, incorporation of Anap in the acid-pocket region may cause some steric hindrance that disrupts mambalgin-1 binding, leading to different desensitization effects and possibly even different IC_{50} values. At the same time, the observed pronounced Anap fluorescence intensity attenuation of the channel labeled at the D347Anap site upon increasing mambalgin-1 (Fig. 2C, 2D) suggests that this site might be in or close to the toxin binding site. In this case, mambalgin-1 binding could cause a change in the environment of the D347Anap label, resulting in the spectral changes (Fig. 2C). Only minor Anap fluorescence intensity attenuation was observed at the T236Anap site in the absence or presence of 500 nM toxin (Fig. 2B), indicating that this site is distant from the toxin binding region.

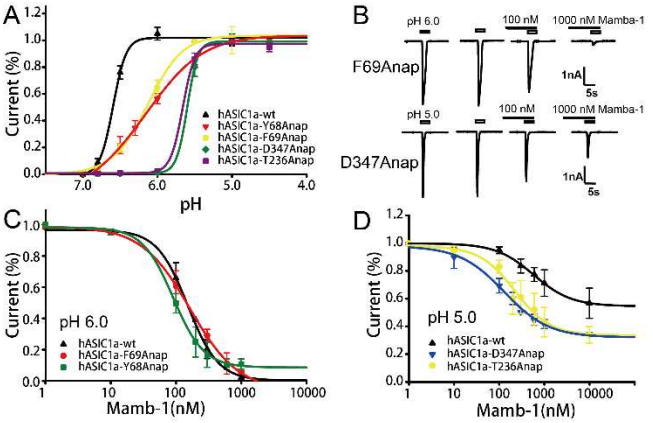

Figure 4. Electrophysiological characterization of wild type and mutant hASIC1a channels in response to different pH and toxin concentrations. (A) Channel conductance measurements of wild type or Anap incorporated hASIC1a channels at different pH. The pH responses were fitted to the Hill equation. The pH gating mid-points were calculated as 6.59 ± 0.02, 6.13 ± 0.04, 6.20 ± 0.06, 5.60 ± 0.12, 5.66 ± 0.05 for hASIC1a WT (n = 4), F69Anap (n = 5), Y68Anap (n = 6), D347Anap (n = 4) and T236Anap (n = 4), respectively. (B) Conductance traces of the hASIC1a-F69Anap, hASIC1a-D347Anap channel inhibitory effect in the presence of 100 nM and 1000 nM mambalgin-1. To exemplify the channel attenuation, the channel conductance was measured under channel open conditions (i.e. hASIC1a-Y68Anap, F69Anap were measured at pH 6.0, while hASIC1a-T236Anap and D347Anap were measured at pH 5.0). (C) The dose-response of channel conductance measurements at different mambalgin-1 concentrations at pH 6.0. IC50 values were calculated as 150.87 ± 17.58 nM for hASIC1a-WT (n = 5), 163.33 ± 28.30 nM for hASIC1a-F69Anap (n = 4), and 90.09 ± 11.02 nM for hASIC1a-Y68Anap (n = 4). (D) The dose-response of channel conductance measurements at different mambalgin-1 concentrations at pH 5.0. IC50 values were calculated as 580.20 ± 190.47 nM for hASIC1a WT (n = 4), 128.48 ± 38.12 nM for hASIC1a-D347Anap (n = 4) and 220.65 ± 80.70 nM for hASIC1a-T236Anap (n = 5).

Conclusions

In a summary, the synthesis of Anap was optimized to make use of the readily available compound 2-bromonaphthalene, resulting in an improved yield under mild conditions. Following standard procedures of UAA incorporation, Anap fluorescence spectra were acquired using an additional prism-based monochromator prior to emission data collection using two-photon excitation fluorescent confocal microscopy. With this instrument, changes in protein conformation or the environment of the labeled sites were probed. Residues in the acid-pocket and TM-1 regions were investigated in the absence and presence of mambalgin-1. Anap fluorescence data were combined with electrophysiological measurements on wild type and labeled proteins. These results revealed differences in the conformational changes in the toxin binding and channel pore regions upon mambalgin-1 binding. Therefore, combinations of the fluorescence spectra analysis with genetically incorporated small-size fluorescence UAA and electrophysiology studies can be used to investigate the molecular mechanisms underlying eukaryotic ion channel properties in a site-specific manner in live mammalian cells.

Notes and references

Hefei National Laboratory for Physical Sciences at the Microscale and School of Life Sciences, University of Science and Technology of China, Hefei 230026 , Anhui, P.R.China. Email: zlhustc@ustc.edu.cn, cltian@ustc.edu.cn

‡These authors contributed equally to this work

† Electronic Supplementary Information (ESI) available: Detailed experimental methods. See DOI: 10.1039/c000000x/

1 B. N. Giepmans, S. R. Adams, M. H. Ellisman and R. Y. Tsien, *Science*, 2006, **312**, 217.
2 I. R. Correa, Jr., *Current opinion in chemical biology*, 2014, **20**, 36.
3 (a) C. Stadler, E. Rexhepaj, V. R. Singan, R. F. Murphy, R. Pepperkok, M. Uhlen, J. C. Simpson and E. Lundberg, *Nature methods*, 2013, **10**, 315; (b) Z. Hao, S. Hong, X. Chen and P. R. Chen, *Accounts of chemical research*, 2011, **44**, 742.
4 (a) A. Chatterjee, J. Guo, H. S. Lee and P. G. Schultz, *Journal of the American Chemical Society*, 2013, **135**, 12540; (b) H. S. Lee, J. Guo, E. A. Lemke, R. D. Dimla and P. G. Schultz, *Journal of the American Chemical Society*, 2009, **131**, 12921.
5 (a) J. Wang, J. Xie and P. G. Schultz, *Journal of the American Chemical Society*, 2006, **128**, 8738; (b) B. E. Cohen, T. B. McAnaney, E. S. Park, Y. N. Jan, S. G. Boxer and L. Y. Jan, *Science*, 2002, **296**, 1700.
6 P. Shi, D. Li, H. Chen, Y. Xiong, Y. Wang and C. Tian, *Protein Sci*, 2012, **21**, 596.
7 (a) J. Kusch and G. Zifarelli, *Biophysical journal*, 2014, **106**, 1250; (b) A. Cha and F. Bezanilla, *Neuron*, 1997, **19**, 1127.
8 (a) G. Bonifacio, C. I. Lelli and S. Kellenberger, *The Journal of general physiology*, 2014, **143**, 105; (b) C. J. Passero, S. Okumura and M. D. Carattino, *The Journal of biological chemistry*, 2009, **284**, 36473.
9 T. Kalstrup and R. Blunck, *Proceedings of the National Academy of Sciences of the United States of America*, 2013, **110**, 8272.
10 (a) K. A. Sluka, O. C. Winter and J. A. Wemmie, *Current opinion in drug discovery & development*, 2009, **12**, 693; (b) R. Waldmann, G. Champigny, F. Bassilana, C. Heurteaux and M. Lazdunski, *Nature*, 1997, **386**, 173.
11 (a) S. Diochot, A. Baron, M. Salinas, D. Douguet, S. Scarzello, A. S. Dabert-Gay, D. Debayle, V. Friend, A. Alloui, M. Lazdunski and E. Lingueglia, *Nature*, 2012, **490**, 552; (b) J. A. Wemmie, R. J. Taugher and C. J. Kreple, *Nature reviews. Neuroscience*, 2013, **14**, 461.
12 (a) C. I. Schroeder, L. D. Rash, X. Vila-Farres, K. J. Rosengren, M. Mobli, G. F. King, P. F. Alewood, D. J. Craik and T. Durek, *Angewandte Chemie*, 2014, **53**, 1017; (b) M. Pan, Y. He, M. Wen, F. Wu, D. Sun, S. Li, L. Zhang, Y. Li and C. Tian, *Chemical communications*, 2014, **50**, 5837.
13 M. Salinas, T. Besson, Q. Delettre, S. Diochot, S. Boulakirba, D. Douguet and E. Lingueglia, *The Journal of biological chemistry*, 2014, **289**, 13363.
14 R. B. Girdler, P. H. Gore and J. A. Hoskins, *J Chem Soc C*, 1966, 518.
15 Z. Xiang and L. Wang, *J Org Chem*, 2011, **76**, 6367.
16 J. Jasti, H. Furukawa, E. B. Gonzales and E. Gouaux, *Nature*, 2007, **449**, 316.
17 I. Baconguis and E. Gouaux, *Nature*, 2012, **489**, 400.